Electronic Supplementary Information (ESI) for

# Reactivity control of a photocatalytic system by changing the light intensity

Christoph Kerzig* and Oliver S. Wenger*

*Department of Chemistry, University of Basel, St. Johanns-Ring 19, 4056 Basel, Switzerland*

## Contents

# 1 General experimental details

## 1.1 Materials

The photocatalyst of our study, trisodium *fac*-tris[2-(5'-sulfonatophenyl)pyridine]iridate(III) pentahydrate (**Irsppy**), was available from our recent investigations, in which it has been prepared and fully characterized.[1,2] All other compounds used for spectroscopy, for lab-scale photoredox reactions or as reference substances were purchased from commercial suppliers and used as received (4-bromo-2-chloro-5-fluorobenzoic acid, 98 %, Combi-Blocks; *trans*-cinnamic acid, 99 %, Aldrich; *trans*-4-fluorocinnamic acid, 99 %, Aldrich; *trans*-3-fluorocinnamic acid, 98 %, Apollo; fumaric acid, ≥ 99 %, Aldrich; maleic acid, ≥ 99 %, Aldrich; succinic acid, ≥ 99 %, Aldrich; 4-(bromomethyl)benzoic acid, 97 %, Aldrich; 4-(chloromethyl)benzoic acid, 98 %, Combi-Blocks; *p*-toluic acid, 98 %, Aldrich; triethanolamine, ≥ 99 %, Aldrich; disodium 1,5-naphthalenedisulfonate hydrate, > 98 %, TCI; trifluoroacetic acid, 99 %, Fluorochem; sodium hydrogen phosphate, > 99 %, Aldrich; sodium dihydrogen phosphate, > 99 %, Aldrich; sodium hydroxide, 98 %, Acros; sodium deuteroxide solution, 40 wt. % in $D_2O$, Aldrich; $D_2O$, 99.9 % deuteration, Cambridge Isotope Laboratories).

Unless otherwise indicated, the solvent was ultrapure Millipore MilliQ water (specific resistance, 18.2 MΩ cm). The pH values were adjusted either with sodium hydroxide or with a freshly prepared phosphate buffer. All solutions used for spectroscopy and photocatalysis were purged with argon (4.8, PanGas) for at least five minutes before the experiments and sealed under argon (1 atm) using cuvettes with septum caps provided by Starna (see Scheme 1 of the main paper and Fig. S3).

## 1.2 Equipment and methods

The complete photochemical characterization of **Irsppy** employing steady-state and time-resolved spectroscopic techniques has been reported recently.[1,2] The pertinent photocatalyst properties are summarized in Section 2 of the main paper.

The kinetic transient absorption (TA) trace displayed in Scheme 1 of the main paper, which displays the lifetime of $^3$**Irsppy**, was recorded with an LP920-KS spectrometer from Edinburgh Instruments at a detection wavelength of 367 nm upon excitation of a diluted argon-saturated **Irsppy** solution with 430 nm laser pulses (~10 ns duration). A more precise description of that laser setup can be found in the next subsection.

Emission lifetime and quenching investigations were carried out with a LifeSpec II setup (Edinburgh Instruments), which is based on the time-correlated single photon counting technique. A picosecond pulsed diode laser (*ca.* 60 ps pulse width) was used for excitation of **Irsppy** at 405 nm. The **Irsppy** concentrations for these lifetime measurements were between 40 and 60 μM. NaOH was added in high concentrations to the aqueous **Irsppy** solutions (final NaOH concentration, 50 mM) to ensure (i) a quasi-constant ionic strength, and (ii) fast

dissolution of the neutral quencher molecules and their dissociation into water-soluble ionic forms.

All spectroscopic experiments presented in this study were carried out at 293 K.

Details concerning our preparative photoirradiation setup and NMR product analyses are given in Chapter 3.

### 1.3 Two-pulse laser flash photolysis

Hydrated electrons for spectroscopic investigations were produced from aqueous **Irsppy** solutions using an LP920-KS apparatus from Edinburgh Instruments. Primary excitation of **Irsppy** was carried out by a Quantel Brilliant laser equipped with an OPO from Opotek using 430 nm as excitation wavelength (typical pulse energies, 8 to 13 mJ). Secondary excitation of $^{3}$**Irsppy** generated by the first pulse was achieved with a second Nd:YAG laser (Quantel Brilliant b, *ca.* 10 ns pulse width) operating at 532 nm; lasers and detection system were synchronized as described earlier.[3] More information on how to achieve homogeneous excitation using beam expanders, laser beam adjustment and laser intensity control can be found in recent studies that employed our two-pulse laser flash photolysis setup.[1,4,5]

Fig. S1 displays representative experiments on argon-saturated **Irsppy** solutions with the above-mentioned laser setup recording kinetic emission (upper panel) and transient absorption (lower panel) traces. The first (blue) laser pulse excites **Irsppy** into its emissive triplet state, which can be selectively monitored through its characteristic and long-lived ($\tau_0$ = 1.6 μs) phosphorescence peaking at ~510 nm. The second (green) pulse with a 240 ns time delay does not excite **Irsppy** as the ground state of our catalyst only absorbs below 500 nm.[2] However, the second pulse efficiently excites $^{3}$**Irsppy** into a higher triplet state thereby inducing photoionization to yield the superreductant $\mathbf{e_{aq}}^{\bullet-}$ and the oxidized catalyst **Irsppy**$^{\bullet+}$. This ionization process manifests itself by a second-pulse induced $^{3}$**Irsppy** bleach (see upper panel in Fig. S1, $t$ = 240 ns), and by the simultaneous formation of the ionization products as monitored by transient absorption spectroscopy (lower panel in Fig. S1). The absorption trace in Fig. S1 was recorded at a wavelength where the interconversion of **Irsppy** and $^{3}$**Irsppy** does not yield any signals, because the superposition of $^{3}$**Irsppy** absorption (positive TA signal) and emission (negative TA signal) is zero at this so-called "pseudo"-isosbestic point. Compared to our recent TA measurements, the position of this "pseudo"-isosbestic point changed from 665 nm (ref. [2]) to 625 nm (Fig. S1 of this study), because the absorption-to-emission sensitivity ratio increased resulting from a recent detection lamp replacement (*i.e.*, the laser flash photolysis setup provides significantly more detection light than before this replacement). For more details concerning the photoionization mechanism and the identification of the ionization products, $\mathbf{e_{aq}}^{\bullet-}$ and **Irsppy**$^{\bullet+}$, we refer to our previous publication[2].

The $\mathbf{e_{aq}}^{\bullet-}$ absorption traces shown in the main paper visualizing either its unquenched lifetime in our system (1.4 μs, Scheme 1) or its reactivity towards 4-(chloromethyl)benzoate (Fig. 3) were basically measured as shown in Fig. S1, but we reduced the interpulse delay to

30 ns (for better visibility of both pulses, a delay of 240 ns was employed for the measurements of Fig. S1) and a significantly higher intensity of the second laser was applied to the system. These two experimental modifications ensure the generation of higher $\mathbf{e_{aq}^{\bullet-}}$ concentrations with the concomitant sensitivity increase of the kinetic TA measurements. Moreover, we removed the TA signals derived from $\mathbf{Irsppy^{\bullet+}}$, which is straightforward (subtraction of a constant offset) given that $\mathbf{Irsppy^{\bullet+}}$ is completely stable on the timescales of our spectroscopic measurements.[2]

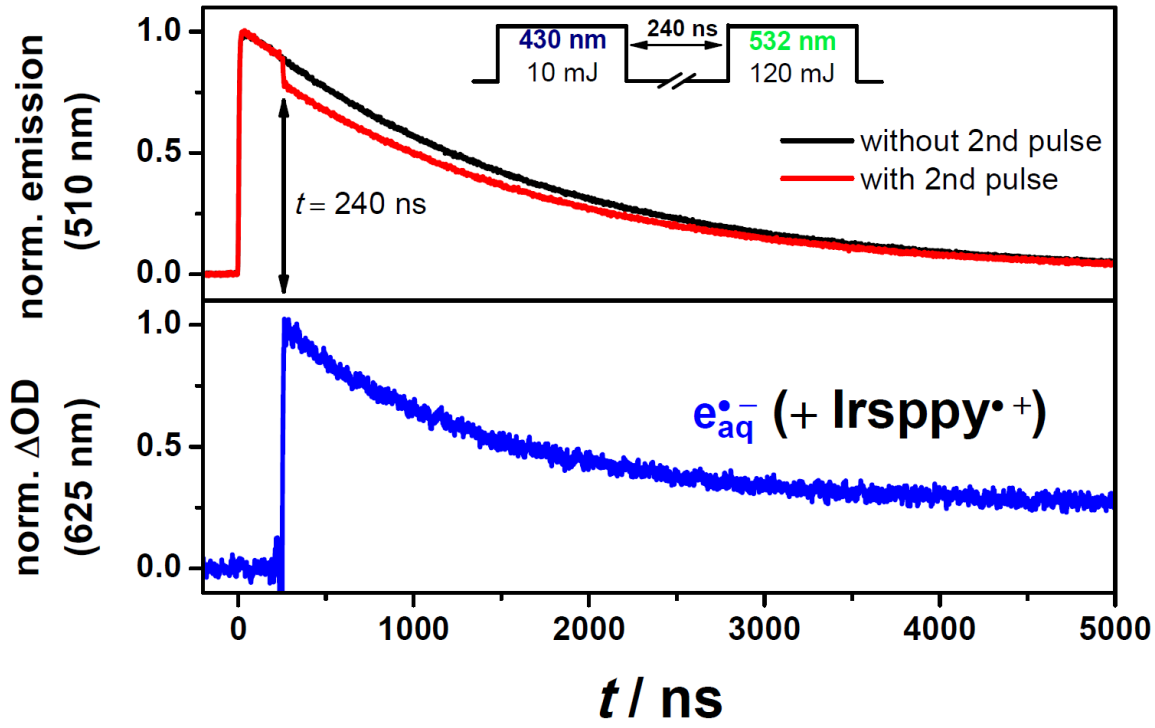


***Fig. S1***: Producing hydrated electrons from **Irsppy** via its triplet ($^3$**Irsppy**) using two-pulse laser flash photolysis) on an argon-saturated aqueous solution containing 50 µM **Irsppy** at pH 12, with the pulse scheme given in the upper panel above the traces. Shown are kinetic emission traces monitoring $^3$**Irsppy** (upper panel) and a kinetic absorption trace at the "pseudo"-isosbestic point of **Irsppy** and $^3$**Irsppy** (625 nm) detecting the photoionization products. For further explanations, see text.

## 2 Additional mechanistic investigations and control experiments

### 2.1 Energy transfer quenching

Our initial substrate for energy transfer reactions was *trans*-cinnamate (see Section 2.1 of the main paper for details). The TCSPC measurements on the *trans*-cinnamate induced $^3$**Irsppy** quenching are displayed in the main plot of Fig. S2. The rate constant determination for the TTET reaction, $^3$**Irsppy** + *trans*-cinnamate $\xrightarrow{k_{\text{trans}}}$ **Irsppy** + $^3$*trans*-cinnamate, is presented in the inset of Fig. S2.

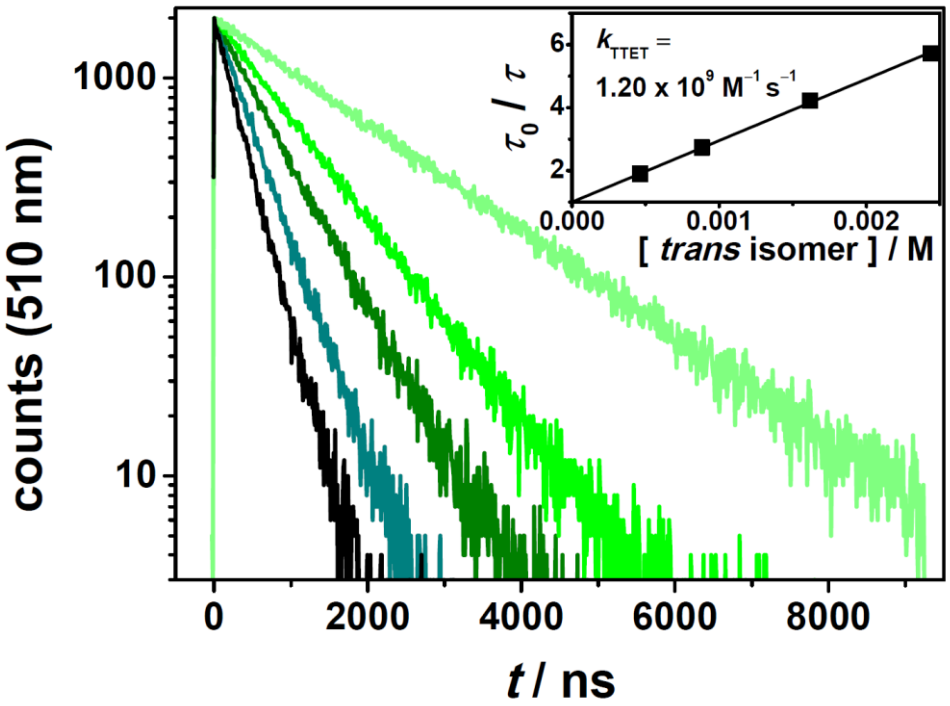


***Fig. S2***: Main plot, emission decay of $^3$**Irsppy** in the absence of *trans*-cinnamate (light green trace) and with *trans*-cinnamate (other traces) after 405 nm excitation of an argon-saturated aqueous solution (60 μM **Irsppy**, pH 12.7). Inset, corresponding Stern–Volmer plot and resulting TTET rate constant.

The widely accepted mechanism for triplet sensitized olefin isomerizations is as follows: The locally excited triplet state, $^3$*trans*-cinnamate in our case, rapidly converts to a lower lying triplet state with a perpendicular structure, which can also be populated from the respective triplet of the other isomer. Subsequently, the ground states of both the *cis* and the respective *trans* isomer are accessible by the relaxation of this perpendicular state.[6,7] The relative concentrations of both geometrical isomers in the photoequillibrium strongly depend on the energies of both locally excited triplet states, with *cis* triplets being typically higher in energy. Because these triplet energies are reflected in the TTET kinetics, we also estimated the energy transfer rate with *cis*-cinnamate as triplet energy acceptor.

Rather than isolating several tens of milligrams of the pure *cis* isomer, we measured the $^3$**Irsppy** lifetime change employing the isomeric mixture present after reaching the photoequilibrium (21% *trans* and 79% *cis*, we could not detect any cinnamate-derived side products, see main paper and Section 3.3 for details) as quencher and extracted the desired rate constant for TTET with *cis*-cinnamate ($k_{cis}$) with the already known $k_{trans}$ (see Fig. S2). Setting up and rearranging the photokinetic equations for the competitive $^3$**Irsppy** quenching in the usual way leads to eqn. (1),

$$k_{cis} = \frac{\frac{1}{\tau_{eq}} - \frac{1}{\tau_0} - k_{trans}\ [trans\,]}{[cis\,]} \qquad (1)$$

Inserting the measured lifetimes (unquenched lifetime $\tau_0$ = 1623 ns and lifetime with the isomeric mixture as quencher $\tau_{eq}$ = 1192 ns) and respective isomer concentration (with the

weight-in concentration, 0.459 mM) into eqn. 1 gives a TTET rate constant for the reaction $^3$**Irsppy** + *cis*-cinnamate $\xrightarrow{k_{cis}}$ **Irsppy** + $^3$*cis*-cinnamate of 3.0 × $10^8$ $M^{-1}$ $s^{-1}$. Almost the same rate constant (3.2 × $10^8$ $M^{-1}$ $s^{-1}$) was obtained at a higher weight-in concentration of unsubstituted cinnamate indicating the reliability of our indirect approach.
Similar results have been obtained for 3-fluorocinnamate (they are summarized in Section 2.2 of the main paper) using the same methodology as for unsubstituted cinnamate.

Studies on the TTET kinetics of the reaction between $^3$**Irsppy** and fumarate were unsuccessful. Employing fumarate as quencher at concentrations up to 20 mM, we did not observe any noticeable $^3$**Irsppy** lifetime decrease, which allows us to estimate an upper limit for the TTET rate constant of ~1 × $10^5$ $M^{-1}$ $s^{-1}$. This limit is in line with kinetic simulations, which predict a TTET rate constant of 6 × $10^4$ $M^{-1}$ $s^{-1}$ when we assume an uphill energy transfer with a $\Delta E$ of 22 kJ $mol^{-1}$ ($\Delta E$ was estimated using the triplet energy of the structurally strongly related dimethyl fumarate)[8] and a Coulomb-reduced diffusion rate of 5 × $10^8$ $M^{-1}$ $s^{-1}$ between a trianion (sensitizer) and a dianionic quencher in water.[6,9,10] However, the lab-scale isomerization reaction proceeds, albeit with a slow reaction rate (see Section 2.2 of the main paper). These observations are in agreement with very recently published studies on endergonic triplet sensitized photoreactions.[11]

**2.2 Electron transfer quenching kinetics**

Our sacrificial donor TEOA used to recover **Irsppy** from its oxidized form **Irsppy**$^{\bullet+}$ does not reductively quench $^3$**Irsppy** even at the high concentrations employed during lab-scale photoredox reactions, which we validated in our recent investigation on the **Irsppy** ionization mechanism (Fig. S5 in ref. [2]).
With our substrate for the dehalogenation studies presented in Section 2.1 of the main paper – 4-bromo-2-chloro-5-fluorobenzoate – we observed very slow $^3$**Irsppy** quenching kinetics. When we employ 4-bromo-2-chloro-5-fluorobenzoate concentrations as high as 30 mM (close to the solubility limit in our aqueous solution containing 50 mM NaOH), the $^3$**Irsppy** lifetime ($\tau_0$ = 1630 ns) is reduced by merely 25 ns, as observed by TCSPC measurements. Together with additional kinetic emission measurements at lower quencher concentrations, a quenching rate constant for the $^3$**Irsppy** driven 4-bromo-2-chloro-5-fluorobenzoate reduction (with subsequent debromination) of ~3 × $10^5$ $M^{-1}$ $s^{-1}$ was estimated from a Stern–Volmer analysis. An even lower quenching rate constant for the less activated 2-chloro-5-fluorobenzoate (and its subsequent dechlorination, compare Fig. 1 of the main paper) is expected. These results and considerations are in accordance with the long reaction times required for the one-photon reaction (Fig. 1 of the main paper) as well as its good selectivity for the debromination product.

## 3 Application-related details

### 3.1 Irradiation setup

A photograph of our setup for photocatalytic lab-scale reactions is displayed in Fig. S3. We employed a 447 nm diode laser from Roithner Lasertechnik (component 1 in Fig. S3) with adjustable power supply (up to 1000 mW optical output), and used its unmodified laser beam (5.0 × 2.5 mm) for the so-called one-photon reactions carried out in this study. The photon flux per area under these conditions amounts to ~8 W $cm^{-2}$ when the laser operates at its maximum output. This power density enables efficient excitation of **Irsppy** to $^{3}$**Irsppy**, but does not permit the biphotonic **Irsppy** ionization producing highly reducing $\mathbf{e_{aq}}^{\bullet-}$.[2]
The incorporation of an inexpensive converging lens ($f$ = 60 mm, LB4592, Thorlabs; component 2 in Fig. S3) between cw laser and cuvette results in a tiny "pseudo-collimated" laser beam over a length comparable to the dimensions of a 10 mm cuvette (component 3 in Fig. S3). This modification greatly increases the power density in the illuminated reaction volume (to about 1 kW $cm^{-2}$)[2] such that the two-photon mechanism liberating $\mathbf{e_{aq}}^{\bullet-}$ can operate efficiently.

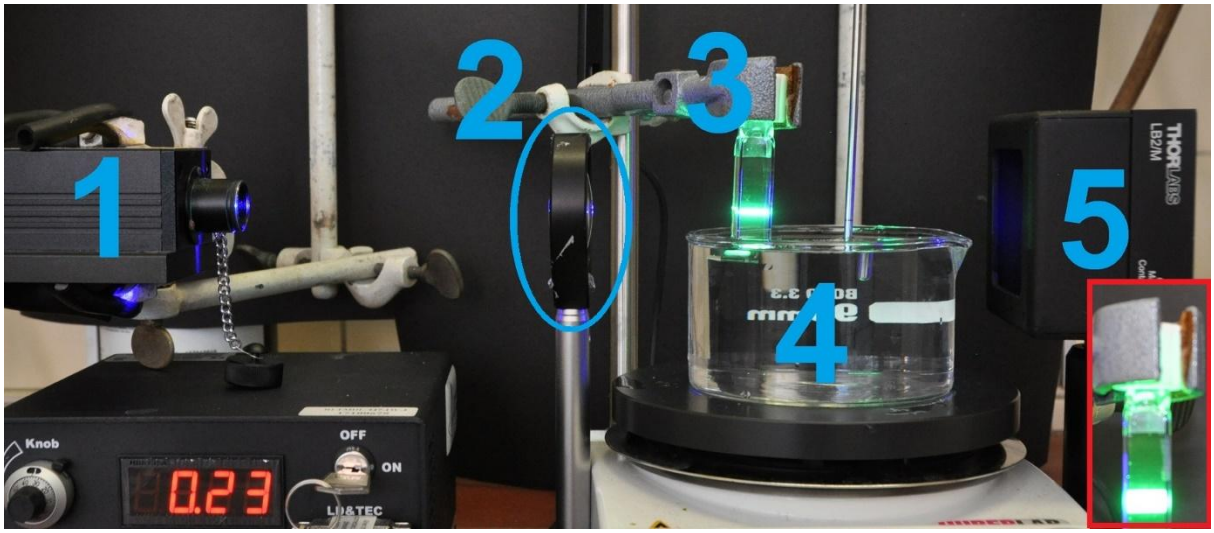


***Fig. S3***: Illumination setup for lab-scale reactions with our catalytic system (compare, scheme 1 of the main paper). 1, cw laser; 2, lens for beam collimation (not used for "one-photon" reactions initiated by $^{3}$**Irsppy**); 3, septum-cap cuvette with stirring bar (and 3 mL of an aqueous **Irsppy** solution); 4, water bath for cooling of illuminated solution; 5, beam block. To visualize the laser beam by the catalyst luminescence, the laser power was reduced to about 15 % of its maximum value. The inset shows a photograph of the cuvette when the lens is omitted, *i.e.*, with the unmodified cw laser beam. Further details are given in the text.

All preparative irradiation experiments were carried out at room temperature (299 ± 2 K) under continuous stirring of the illuminated solutions using a small magnetic bar (Fig. S3). Heating of the solutions during irradiation was avoided by dipping the lower part of the cuvette into a water bath (component 4, room temperature water without additional cooling was used). That simple procedure ensured that the temperature of the irradiated solution did not exceed 304 K. Moreover, a beam block (component 5 in Fig. S3) was used for safety reasons.

### 3.2 Analytical methods

Identification and concentration determination of photoproducts was carried out by NMR spectroscopy with a Bruker Avance III spectrometer operating at a proton frequency of 400 MHz. All spectra were measured at 295 K, and chemical shifts were referenced to the solvent peak ($^1$H NMR, $D_2O$, $\delta = 4.79$ ppm)[12] or to trifluoroacetate ($^{19}$F NMR, TFA, $\delta = -76.2$ ppm)[13]. All photoirradiation experiments were carried out with the setup described in Section 3.1 using argon-saturated solutions. The pH values of all solutions used for illumination experiments were between 12 and 12.7 to keep all carboxylic acids in their deprotonated water-soluble forms.

### 3.3 Reductive dehalogenations

The photoreactions with the substrate 4-bromo-2-chloro-5-fluorobenzoate were carried out in $H_2O$. Sample workup was carried out by adding $D_2O$ (10% v/v, for shimming and locking) containing well-defined trifluoroacetate concentrations. Trifluoroacetate served not only as internal standard, but also as reference for quantifications. The results of the quantitative $^{19}$F NMR experiments (carried out with proton decoupling) on the one- and two-photon reactions with 4-bromo-2-chloro-5-fluorobenzoate reactions are displayed in Fig. 1 of the main paper. The wide chemical shift range of $^{19}$F NMR spectroscopy with clearly distinguishable signals for structurally very similar compounds,[14] together with previous $^{19}$F NMR studies on 3-fluorobenzoate as well as 2-chloro-5-fluorobenzoate,[15,16] ensured unambiguous identification of our photoproducts.

The debromination selectivity parameter of the one-photon reaction (which amounts to 62, see main paper) was calculated from the 2-chloro-5-fluorobenzoate–to–3-fluorobenzoate ratio obtained from $^{19}$F NMR integrals.

The reaction mixture after the two-photon reaction (100% conversion, see Fig. 1c of the main paper) contains the two-fold dehalogenated compound 3-fluorobenzoate as main product (60%) and remaining debrominated substrate (2-chloro-5-fluorobenzoate, 33%). Moreover, low fluoride ion ($\delta = -120.3$ ppm)[2,17] concentrations corresponding to about 2.5% defluorination could be detected in the $^{19}$F NMR spectrum after irradiation with the two-photon setup. This observation suggests that a hydrated electron induced defluorination[17] of 3-fluorobenzoate to yield benzoate might occur. However, this defluorination reaction seems to be significantly slower than with the *para*-isomer (4-fluorobenzoate),[17] which allowed us to obtain the two-fold dehalogenated compound as main product with a dechlorination(60%)–to–defluorination(2.5%) selectivity of 24 under our conditions. Further side products could not be identified.

### 3.4 Isomerization vs. hydrogenation

As the $^1$H NMR spectra in Fig. S4 illustrate, irradiation of *trans*-cinnamate with our one-photon setup resulted in an isomeric mixture with the *cis* isomer as main product (see figure caption for reaction conditions). The $^1$H NMR data presented in ref. [18] confirm this

isomerization. The water-soluble reference compound 1,5-naphthalenedisulfonate (NDS)[19] was used for quantification**.** Well-defined amounts of NDS were added in solid form, both to the solution after irradiation and to an aliquot of the non-irradiated solution. Analyzing the NMR integrals, this procedure revealed the following composition of the photoequilibrium (longer irradiation times do not change the yields): 21% *trans*-cinnamate and 79% *cis*-cinnamate.

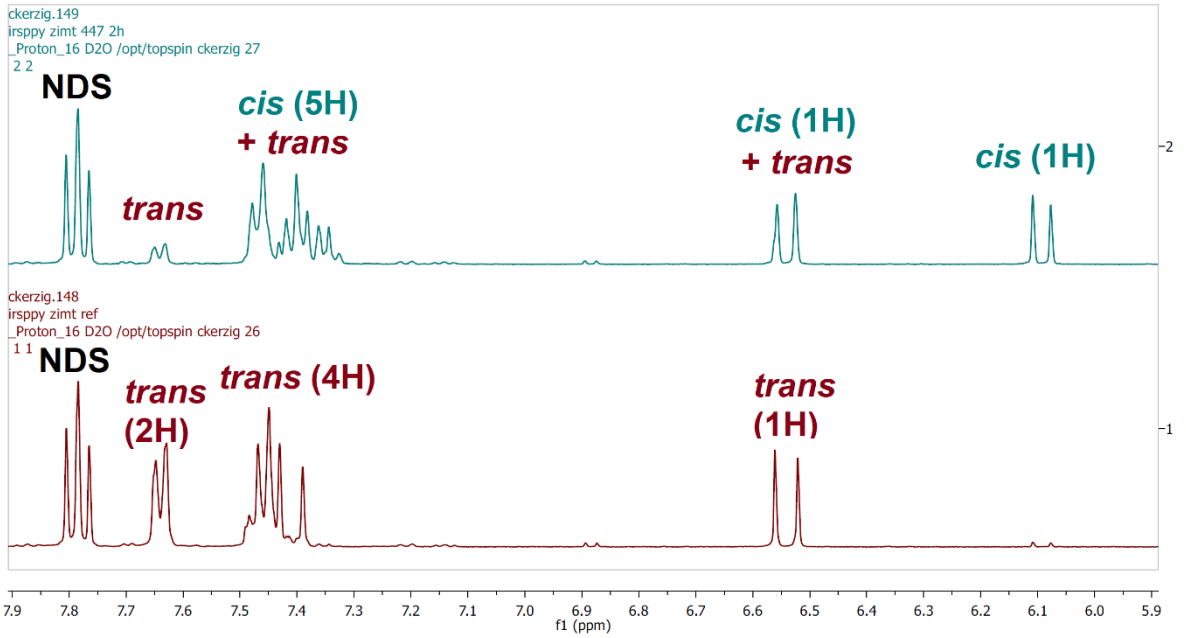


***Fig. S4***: Photoisomerization of *trans*-cinnamate (15 mM in $D_2O$ containing 50 mM NaOD and 2% **Irsppy**). Shown are the $^1$H NMR spectra recorded before (lower panel) and after (upper panel) 2.5 h of blue-light irradiation (447 nm, 1W, "one-photon" setup). The triplet in the aromatic region that does not change is due to 1,5-naphthalene disulfonate (NDS), which was added to quantify the decrease of the *trans* as well as the increase of the *cis* isomer. See text for details.

The photoreaction products with the *trans*-3-fluorocinnamate substrate were identified[15] and analyzed employing $^{19}$F NMR spectroscopy as described in Section 3.3 for 4-bromo-2-chloro-5-fluorobenzoate. The spectra used for the reaction yield determinations are shown in Fig. S5, which display the product regions of the NMR spectra and the TFA reference signals. The two-photon reaction with the hydrogenated main product (62% yield, see Section 2.2 of the main paper) produces also several side products as indicated by additional peaks in the $^{19}$F NMR spectrum (Fig. S5c). However, only the signal at $\delta = -120.3$ ppm, which is due to fluoride ions (7% yield, see also Section 3.3), could be identified. We regard the fluoride ion release as a side reaction initiated by a (slow) $\mathbf{e_{aq}}^{\bullet-}$ induced one-electron reduction of the desired hydrogenated product with subsequent dissociative electron transfer to yield fluoride ions. This is borne out by our results for the *trans*-4-fluorocinnamate two-photon reaction that gave a significantly lower yield of the hydrogenation product and higher fluoride ion concentrations, since the *para* position of the fluoro substituent (compared to *meta* position) results in a faster $\mathbf{e_{aq}}^{\bullet-}$ attack,[20] but should also facilitate the dissociative fluoride release. Despite this undesired reaction competing

with product formation the yield for the two-photon hydrogenation of t*rans*-3-fluorocinnamate is quite good.

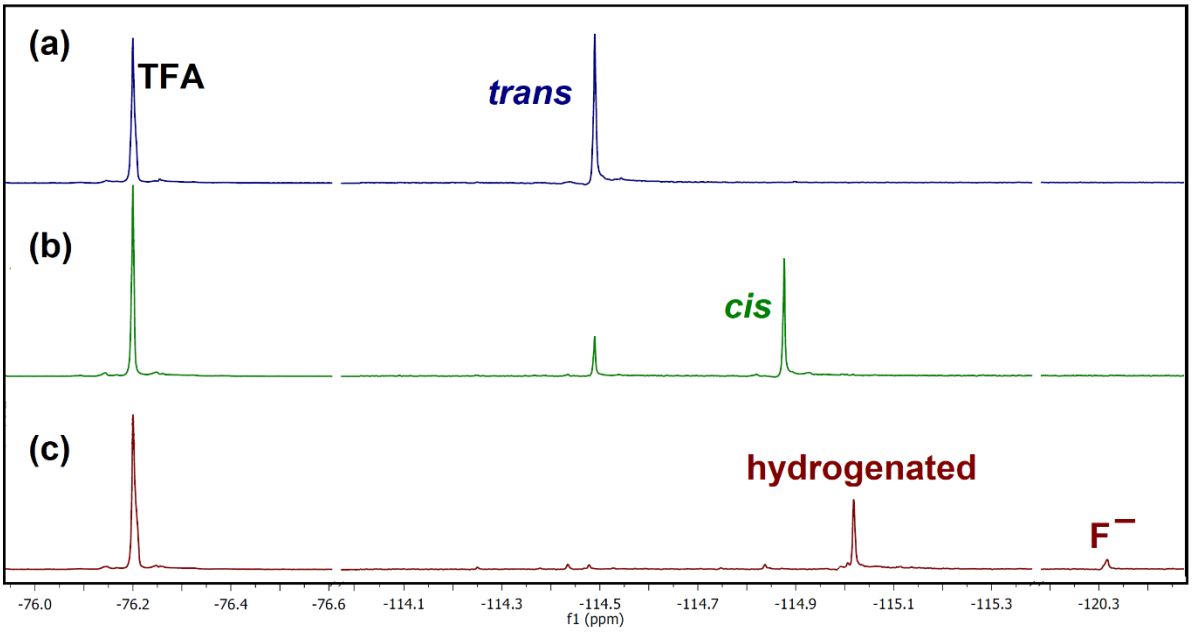


***Fig. S5***: Photoisomerization (with "one-photon" setup, panel (b)) and hydrogenation (with "two-photon" setup, panel (c)) of *trans*-3-fluorocinnamate (under the conditions given at the upper reaction equations in Fig. 2 of the main paper). Shown are the $^{19}$F NMR spectra recorded before (panel (a)) and after (panels (b) and (c)) blue-light irradiation. The signal at –76.2 ppm is due to trifluoroacetic acid (TFA), which was added as reference for quantifications. See text for further explanations.

The $^{1}$H NMR spectra used to determine product yields for the fumarate photoreactions of the main paper (Fig. 2) are displayed in Fig. S6. Also included in this figure are reference spectra showing the expected product signals under identical conditions. Non-deuterated water was employed as solvent ensuring that only hydrogen atoms are added to the intermediates during the two-photon reaction, which avoids analytical problems with isotopic mixtures. Before measuring NMR spectra, $D_2O$ containing NDS as reference (10% v/v) was added for shimming and locking. The intense solvent peaks in the $^{1}$H NMR spectra so obtained do not negatively influence starting material and product signals, as the spectra in Fig. S6 clearly demonstrate.

We observed noticeable succinate concentrations in initial studies on the fumarate photoreaction under one-photon conditions when TEOA was present. However, only traces of the hydrogenation product succinate (< 1%) and good maleate (*cis* isomer) yields could be obtained in the absence of TEOA (left part of Fig. S6).

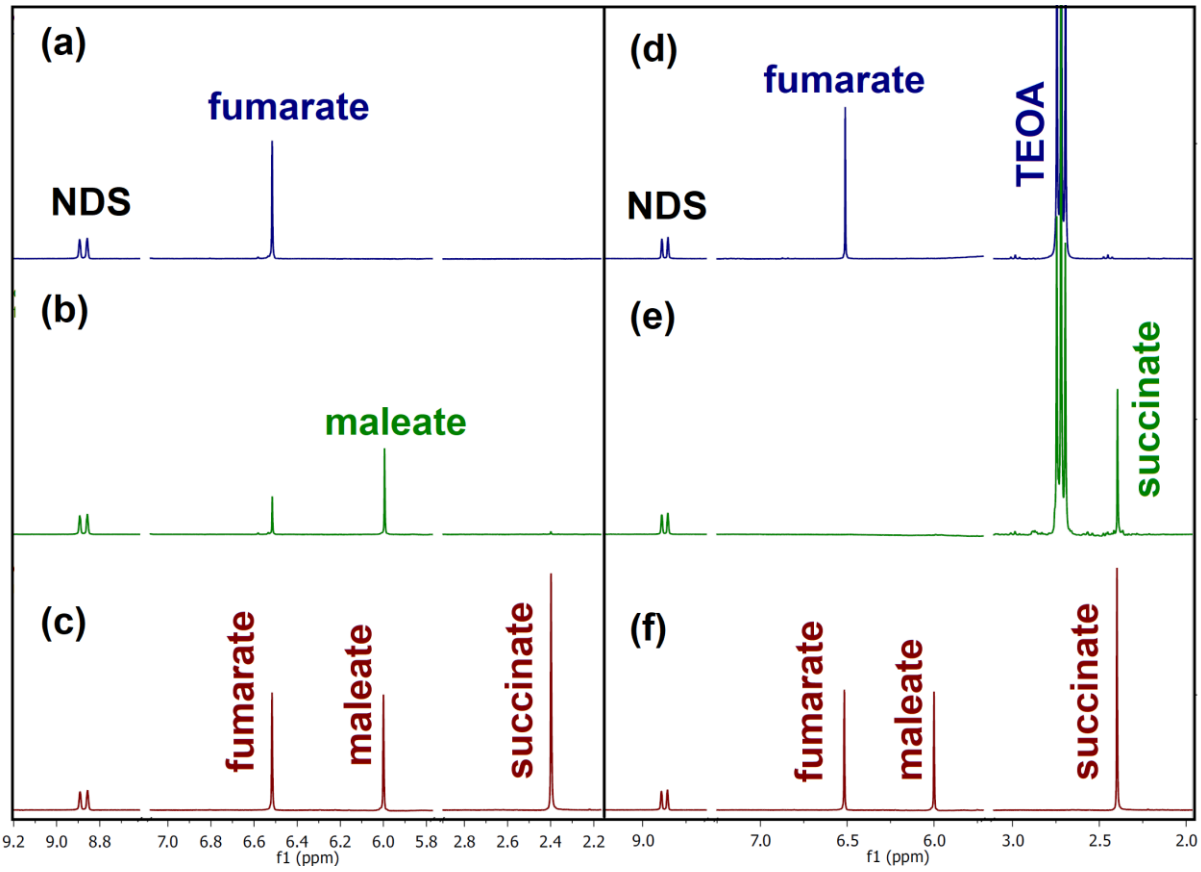


***Fig. S6***: Photoisomerization (with "one-photon" setup, panel (b)) and hydrogenation (with "two-photon" setup, panel (e)) of fumarate (under the conditions given at the lower reaction equations in Fig. 2 of the main paper). Shown are the $^{1}$H NMR spectra recorded before (panels (a) and (d)) and after (panels (b) and (e)) blue-light irradiation, as well as reference spectra (panels (c) and (f)) allowing the unambiguous identification of the photoproducts. The doublet at 8.87 ppm results from 1,5-naphthalene disulfonate (NDS), which was used as reference. For details, see text.

In the case of *trans*-3-fluorocinnamate, no detrimental TEAO effect could be observed when the isomerization was studied under one-photon conditions. This allowed us to use the very same solution for both the one- and the two-photon reaction of that substrate (compare, Fig. 2 of the main paper).

### 3.5 Hydrogen abstraction vs. dimerization

Two novel products can be observed in the aromatic region of the $^{1}$H NMR spectrum upon illumination of 4-(chloromethyl)benzoate (abbreviated as ClBz, Fig. S7). The hydrogen abstraction product could be identified (see Fig. S7 for signal assignment and Fig. 3 of the main paper for reaction equations) with an authentic reference of *p*-toluic acid (4-methylbenzoic acid), whose reference $^{1}$H NMR spectrum was recorded in alkaline $D_2O$. Given the well-established reactivity of benzyl radicals in photoredox catalysis,[21–24] the remaining signals must be ascribed to the dimerization product (see Fig. 3 of the main paper for the structure). Signals of the starting material ClBz and both products can be monitored in isolation allowing straightforward NMR integral analyses. For quantification, we again added

1,5-naphthalenedisulfonate (NDS) as water-soluble internal reference (not shown). That reference was added after recording the spectra displayed in Fig. S7, because the NDS signals partially superimpose the product and ClBz signals in the aromatic region ($\delta$> 7.7 ppm). The color-coded asterisked signals in Fig. S7 were used for yield determinations. Yields and reaction conditions for the 4-(chloromethyl)benzoate photoreactions are given in the main paper (Section 2.3).

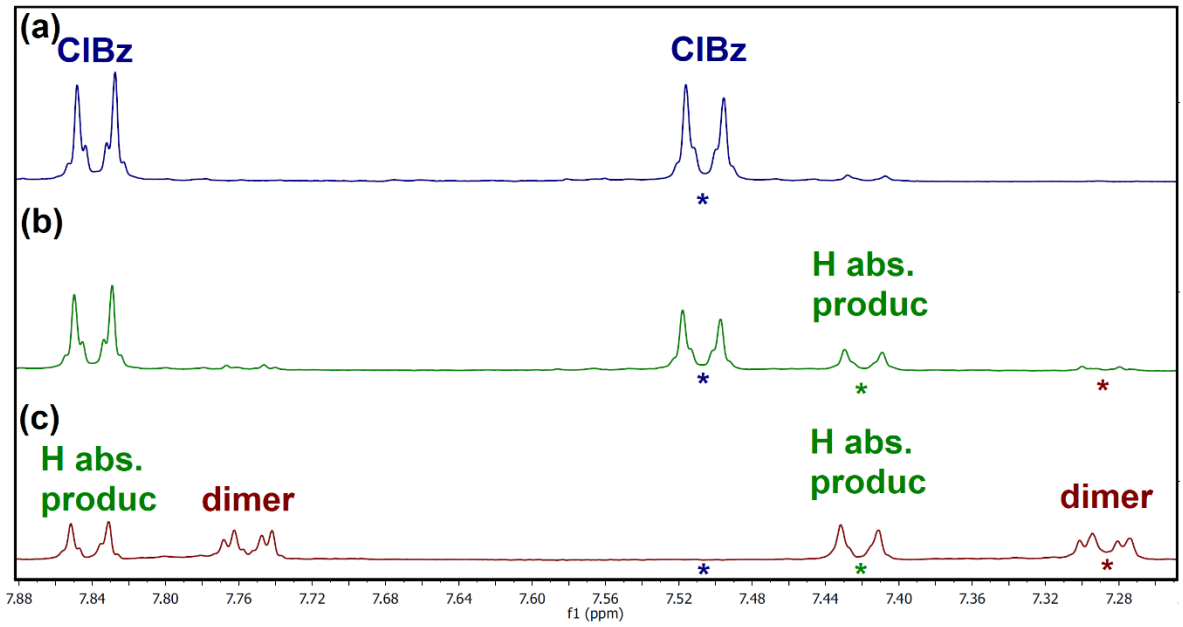


***Fig. S7***: Photoreduction of 4-(chloromethyl)benzoate using the irradiation setup without (panel (b)) and with (panel (c)) the lens for beam collimation under the conditions given at the reaction equations in Fig. 3 of the main paper. The $^{1}$H NMR spectrum of the 4-(chloromethyl)benzoate solution before irradiation is displayed in panel (a). See text for details.

## 4 Supplementary references


1 X. Guo, Y. Okamoto, M. R. Schreier, T. R. Ward and O. S. Wenger, *Chem. Sci.*, 2018, **9**, 5052–5056.

2 C. Kerzig, X. Guo and O. S. Wenger, *J. Am. Chem. Soc.*, 2019, **141**, 2122–2127.

3 M. Kuss-Petermann and O. S. Wenger, *Helv. Chim. Acta*, 2017, **100**, e1600283.

4 S. Neumann, C. Kerzig and O. S. Wenger, *Chem. Sci.*, 2019, **10**, 5624–5633.

5 M. Skaisgirski, C. B. Larsen, C. Kerzig and O. S. Wenger, *Eur. J. Inorg. Chem.*, 2019, DOI:10.1002/ejic.201900453.

6 P. Klán and J. Wirz, *Photochemistry of organic compounds: from concepts to practice*, Wiley, Chichester, West Sussex, U.K., 2009.

7 F. Strieth-Kalthoff, M. J. James, M. Teders, L. Pitzer and F. Glorius, *Chem. Soc. Rev.*, 2018, **47**, 7190–7202.

8 M. J. Mirbach, M. F. Mirbach and A. Saus, *J. Photochem.*, 1982, **18**, 391–393.

9 P. Debye, *Trans. Electrochem. Soc.*, 1942, **82**, 265.

10 C. Kerzig and M. Goez, *Phys. Chem. Chem. Phys.*, 2015, **17**, 13829–13836.

11 F. Strieth-Kalthoff, C. Henkel, M. Teders, A. Kahnt, W. Knolle, A. Gómez-Suárez, K. Dirian, W. Alex, K. Bergander, C. G. Daniliuc, B. Abel, D. M. Guldi and F. Glorius, *Chem.*, 2019, DOI:10.1016/j.chempr.2019.06.004.
12 H. E. Gottlieb, V. Kotlyar and A. Nudelman, *J. Org. Chem.*, 1997, **62**, 7512–7515.
13 F.-F. Zhang, M.-H. Jiang, L.-L. Sun, F. Zheng, L. Dong, V. Shah, W.-B. Shen and Y. Ding, *The Analyst*, 2015, **140**, 280–286.
14 S. Berger, S. Braun and H.-O. Kalinowski, *NMR Spektroskopie von Nichtmetallen, vol. 4, $^{19}$F-NMR-Spektroskopie*, Thieme, Stuttgart, 1994.
15 S. E. Boiadjiev and D. A. Lightner, *J. Phys. Org. Chem.*, 1999, **12**, 751–757.
16 A. Singh, R. P. Sharma, T. Aree and P. Venugopalan, *J. Chem. Sci.*, 2010, **122**, 739–750.
17 R. Naumann, F. Lehmann and M. Goez, *Angew. Chem. Int. Ed.*, 2018, **57**, 1078–1081.
18 M. L. Salum, C. J. Robles and R. Erra-Balsells, *Org. Lett.*, 2010, **12**, 4808–4811.
19 M. Brautzsch, C. Kerzig and M. Goez, *Green Chem.*, 2016, **18**, 4761–4771.
20 G. V. Buxton, C. L. Greenstock, W. P. Helman and A. B. Ross, *J. Phys. Chem. Ref. Data*, 1988, **17**, 513–886.
21 C. B. Larsen and O. S. Wenger, *Inorg. Chem.*, 2018, **57**, 2965–2968.
22 Y. Zhang, J. L. Petersen and C. Milsmann, *J. Am. Chem. Soc.*, 2016, **138**, 13115–13118.
23 G. Park, S. Y. Yi, J. Jung, E. J. Cho and Y. You, *Chem. - Eur. J.*, 2016, **22**, 17790–17799.
24 T. C. Jenks, M. D. Bailey, J. L. Hovey, S. Fernando, G. Basnayake, M. E. Cross, W. Li and M. J. Allen, *Chem. Sci.*, 2018, **9**, 1273–1278.